Pergamon

Int. J. Heat Mass Transfer. Vol. 41, No. 12, pp. 1821–1831, 1998

Printed in Great Britain
0017–9310/98 $19.00+0.00

PII: S0017–9310(97)00294–9

Dehumidification of air flow through cooling at sub-freezing temperatures

CHRISTOS HOUSIADAS,† KARL-HEINZ SCHRADER and YANNIS DROSSINOS

European Commission, Joint Research Centre, I-21020 Ispra (VA), Italy

(*Received* 18 *March* 1997 *and in final form* 20 *July* 1997)

Abstract—An experimental and numerical study is presented in which laminar air flow with low water-vapour concentration is cooled at temperatures well below 0°C to remove the humidity contained in the carrier gas. The experiment uses a cold trap that consists of a vertical tube-bundle immersed in a cold shell. The analysis is carried out with the help of a model that simulates heat and mass transfer, as well as aerosol dynamics in the tube flow. It is found that an optimal temperature range exists for the efficiency of the process. The results are interpreted in terms of the competition between vapour diffusion to the wall and ice particle formation and growth. © 1998 Elsevier Science Ltd. All rights reserved.

1. INTRODUCTION

The present paper deals with a particular case of the general problem of removing a condensible species from an effluent through cooling. Standard applications of this technique, the so-called cold trapping technique, include the removal of impurities from liquid metals in systems such as fast breeder reactors or fusion Tokamak blankets. For moisture removal, cold trapping has been considered in the last few years in conjunction with tritium technology applications. The technique is contemplated for the purification of gas streams containing tritiated water vapour (HTO).

Very limited work has been reported on water cold trapping [1, 3]. The approach consists of freezing out the entering humidity on the cold heat exchange surfaces under temperature conditions chosen to minimize the residual concentration at the exit. Cryogenic conditions have been applied, on the basis of the sub-ppm equilibrium partial vapour pressure at such temperatures. Previous works deal primarily with the development of the process and the associated equipment to demonstrate the feasibility of the approach. Less focus is given on the analysis of the physical effects that take place. However, their significance on the efficiency of the process may be important. As shown in the present study, the physical situation is somehow counter-intuitive: at very low temperatures a considerable fraction of the water vapour nucleates and condenses onto particles which may escape from trapping. This essential effect was clearly evidenced in previous performance tests, cf. ref. [1], and it is also addressed in ref. [3]; yet, it has not been sufficiently analyzed.

The physical picture of a tube flow undergoing dehumidification through freezing is quite complex, including vapour diffusion to the cold walls and condensation there, homogeneous and/or heterogeneous nucleation of particles, and transport of the formed particles with simultaneous growth and deposition. Numerous studies of aerosol formation and transport in tube flow have been performed, mainly in relation with laminar aerosol generators, or with radioactive aerosols in nuclear reactor safety analyses. In many situations an adequate level of understanding of the physics involved has been achieved (see, for example, refs. [4–6]). It has been demonstrated that the individual processes are strongly temperature dependent and that their rates are mutually competing. Therefore, temperature is expected to be the parameter which predominantly affects the overall net result, i.e., the total efficiency of the process. It is the objective of this investigation to study experimentally and numerically the efficiency of water vapour cold trapping over a wide range of sub-freezing temperatures.

The experimental study is conducted at gas temperatures in the range of 0 to −90°C and flowrates between 0.5 and 1.6 m^3 (STP)/h ($\approx 2.7 \times 10^{-4}$ and 8.5×10^{-4} kg s^{-1}, respectively). The input gas flow is moist air at atmospheric pressure and room temperature, with a low absolute humidity content, equal for the reference case to 1250 ppm (which corresponds to a mass concentration of approximately 1000 mg m^{-3}). This range of parameters is relevant to atmospheric detritiation systems in future fusion power plants. The cold trap used in these experiments was constructed in the form of a shell-and-tube heat exchanger. The purpose here is not necessarily to promote a new design approach, but to provide experimental data

† Present address: National Centre for Scientific Research "Demokritos", P.O. Box 60228, GR-15310 Aghia Paraskevi Attikis, Greece.

NOMENCLATURE

c_p	specific heat at constant pressure [J kg^{-1} °C^{-1}]
C	bulk-average mass concentrations [kg m^{-3}]
Cn	condensation number, $\lambda_g/\mathscr{L}D_v\rho'_{v,sat}$, dimensionless
D	coefficient of diffusion in air [m^2 s^{-1}]
d_h	hydraulic diameter [m]
F	deposited fraction, defined by equations (6)–(7)
I_{coag}	coagulation integral [m^{-4} s^{-1}]
J_{nucl}	nucleation rate [m^{-3} s^{-1}]
L	tube length [m]
$\mathscr{L}$	latent heat of condensation [J kg^{-1}]
Le	Lewis number ($=Sc/Pr$), dimensionless
$\dot{m}$	mass flow rate [kg s^{-1}]
n	particle number distribution function [m^{-4}]
Pr	Prandtl number, dimensionless
r	particle radius [m]
r^*	critical radius [m]
$\dot{r}$	particle growth rate [m s^{-1}]
Sc	Schmidt number, dimensionless
Sh	local Sherwood number, dimensionless
SS	supersaturation ratio, defined by equation (5)
t	time [s]
T	temperature [°C]
v	velocity [m s^{-1}]
X, x	axial coordinate [m].

Greek symbols

δ	Dirac distribution function
λ	coefficient of thermal conductivity [W m^{-1} °C^{-1}]
ρ	density [Kg m^{-3}]
ρ'	derivative with respect to temperature [Kg m^{-3} °C^{-1}].

Subscripts

d	deposition
g	carrier gas (air)
in	inlet section
out	outlet section
p	ice particles
sat	saturation relative to water vapour
t	total
v	water vapour
wall	wall structural surface.

Acronym

STP	Standard Temperature and Pressure.

and assess the modelling approach under realistic geometries.

Since the experimental facility did not allow for very detailed measurements, numerical simulations are also performed in an effort to obtain a better understanding of the significance of the various mechanisms involved in the process. The modelling approach is based on an existing advanced calculation scheme developed by Im and co-workers [7], originally used to analyze transport and deposition of aerosols and vapours in reactor coolant systems. To the authors' knowledge this is the first attempt to compare a numerical simulation model with experimental results on dehumidification at highly sub-freezing temperatures.

2. DESCRIPTION OF THE COLD TRAP

In designing the cold trap emphasis was placed on obtaining a large exchange area in a compact and drainable form. The adopted approach is similar to that found in the classical shell-and-tube heat exchangers. The mechanical design is shown in Fig. 1.

The surface for freezing out the humidity is formed by employing a tube bundle of 57 tubes of 11 mm internal diameter and 183 mm long, providing an exchange area of about 0.4 m^2. The tube bundle is immersed in a cold bath accommodated in a cylindrical shell. The bath is obtained by introducing into the shell a quantity of cryogenic fluid (liquid nitrogen), which is then bled off to the atmosphere through a vertical venting line (see horizontal cross section in Fig. 1). A vacuum tight chamber, evacuated to provide thermal insulation, surrounds the shell. Allowance is made for measuring the temperature at different elevations in the cold bath. For that purpose a top open vertical pocket, spanning the active height of the shell is provided, where temperature sensors are introduced (Fig. 1, points A and B).

After flowing downwards through the bundle, the cooled gas is then forced to reverse direction and flow upwards to the outlet of the device through a single large tube of internal diameter of 24 mm.

Another feature of the trap is the possibility to drain the trapped moisture following removal of the cryogenic liquid. The bottom of the trap is provided with a sloped floor area for collecting the melted ice, which is then drained through opening a manual valve (not shown in the figure), attached on the vertical drainage line.

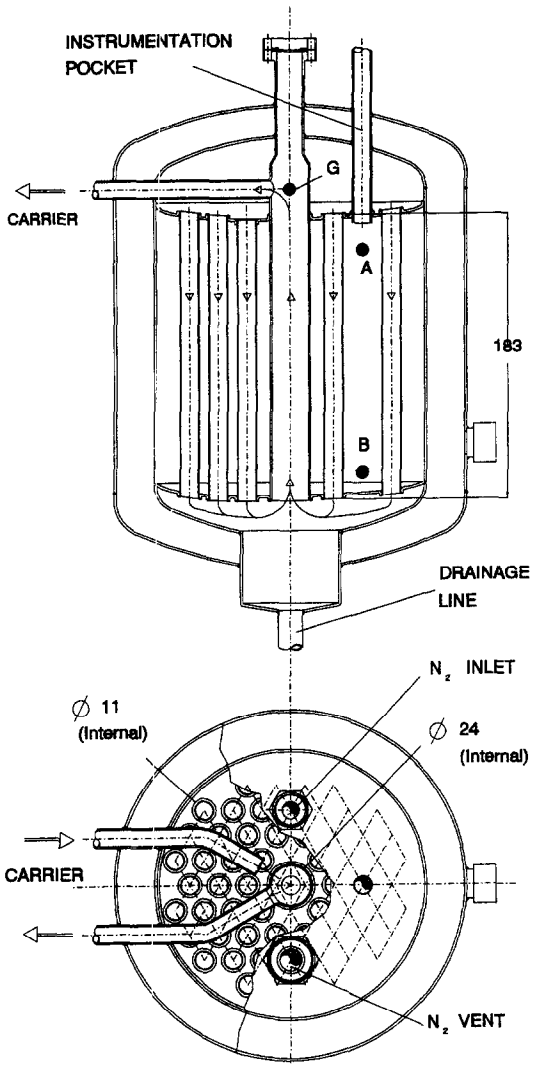

Fig. 1. Mechanical design of the cold trap.

The whole construction is made of stainless steel AISI 304L. All the internal tube surfaces in contact with the flow are of high quality surface finish (electropolished).

3. EXPERIMENTAL

The schematic diagram of the experimental set-up used in the present study is shown in Fig. 2.

The carrier gas flow is provided either from the available compressed air network of the laboratory or from a gas bottle (80% N_2 and 20% O_2 in volume, with impurities <3 ppm), depending on the selection of the experimental conditions. Part of the flow is humidified by passing it through a bubbler containing de-ionized water and then it mixes with the dry stream. The desired water loading at the inlet of the cold trap is obtained by controlling the flowrates of the wet and dry streams. For that purpose two thermal mass flow controllers are employed (of MKS), connected to a multi-channel readout/setpoint device. As discussed before, the water vapour content at the inlet of the cold trap was low (1250 ppm in the reference case). Generally, less than 10% of the total flow was required to be diverted through the bubbler to get the desired inlet humidity.

The water vapour content of the gas (i.e., absolute humidity) is measured with on-line hygrometers equipped with ceramic technology moisture sensors (Cermet series of MICHELL). These instruments cover the range -80 to $+20$°C dew-point ($\approx 0.5-23\,000$ ppm) and have a general accuracy of ± 2°C. The corresponding relative error on the measured humidity concentration is not uniform throughout the whole range (it increases with decreasing humidity). Typically, for the humidity levels encountered in the present experiment, the relative error was of the order of $\pm 20\%$. One hygrometer is located before the bubbler to monitor the humidity of the carrier flow. Two other hygrometers measure the humidity before and after the cold trap. Since the hygrometer sensor may not give representative results if frozen particulates escape with the dried gas from the trap, the exit gas is heated with an electrical heater to about 25°C prior to being presented to the sensor. This approach helps also to preserve the integrity of the sensor, given that its operation is not recommended in environments colder than -20°C. However, there is a disadvantage. The dead space introduced between the sample point and the exit of the cold trap may have an influence on the sensor measurements at low dew-points, due to possible evolution of moisture previously sorbed by the pipe walls. To minimize possible effects, stainless steel is used in this line with high quality surface finish (electropolished). In a separate field test, carried out with an ultra-dry carrier from a gas bottle, the effect was found to be less than 5 ppm (absolute).

The cryogenic fluid is supplied from a liquid nitrogen dewar of a nominal capacity of 0.23 m^3. The dewar is provided with an internal pressure building system which maintains the discharge pressure constant while liquid withdrawal is taking place.

Temperature measurements are performed with platinum resistance thermometers (Pt-100), which have a usable range down to -200°C. The typical sensor tolerance values are 0.3 and 0.8°C at 0 and -100°C, respectively (class B according to DIN 43760). The circuit is instrumented at three locations, as indicated in Fig. 2. The cold trap itself is equipped with three temperature sensors. Two are used to measure the temperature in the shell, while the third measures the exit temperature of the tube flow (Fig. 1, points A, B, G, respectively). Each of these three sensors is contained in a long cartridge, with a metallic sheath of 3.2 mm in diameter to enable their positioning in the interior of the device.

For all tests the inlet humidity, inlet temperature and flow rate were kept constant, while the tem-

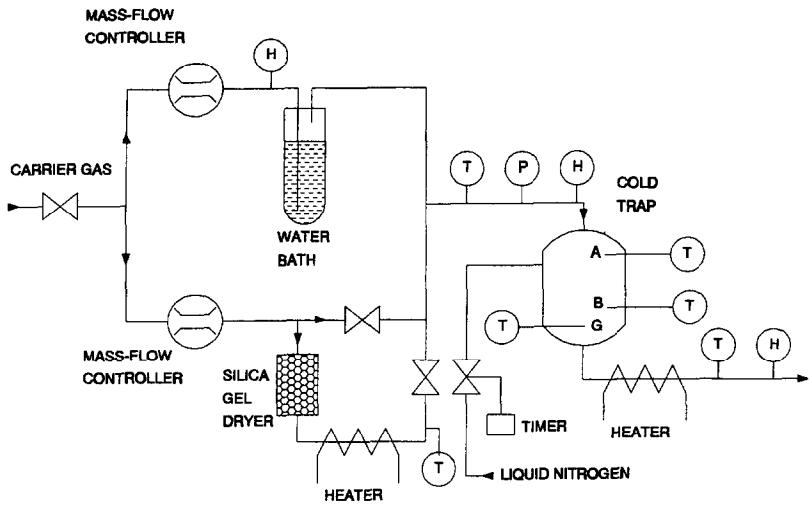

Fig. 2. Schematic of the experimental circuit (T, H, P: measurements of temperature, humidity and pressure, respectively).

perature of the cold bath was varied to obtain different operating temperature conditions. Special care was taken to proceed with slow temperature variations so that the transient takes up the form of a succession of stationary conditions. This has been achieved by employing a simple heuristic approach. The technique consists of introducing the coolant into the shell in a mode of flow pulses with their frequency varying during the run. For this purpose an electromagnetic on/off valve commanded by a timer was mounted at the liquid nitrogen supply line (a special CRYO valve of SIO). A video monitor is connected to the data logger showing, with a scanning period of 1 s, the evolution of temperature and exit dew-point. When steady-state conditions are visualized, the injection pulses are gently increased and a new operating state is established at a lower temperature level. The typical magnitudes of the employed flow pulses are concerned with injections over a period of the order of 200 ms (i.e., duration of the valve opening) at intervals of around 10 s. No attempt was made to analyze these data, the scope being outside the intend of the present study. Finally, it is useful to mention here, that fairly uniform mixing was observed in the shell: in general, the two available temperature measurements at the positions A and B exhibited variances of the order of 10°C.

Prior to any testing, the whole circuit is dried by using the bypass auxiliary arrangement shown in Fig. 2. The air first passes through a silica gel bed, it is then heated to about 60°C with an electrical heater, and it subsequently flows throughout the whole loop in a once-through mode, over a period of some hours. The objective of this sequence was to obtain the same initial moisture loading on all parts of the circuit.

4. MODELLING

The goal of the modelling effort is to provide physical insight on the parameters and conditions that influence the efficiency of the process, as well as to establish a calculation scheme to reproduce the main features of the experimental results. The model consists of two computational cells in series: the first simulates the downward tube-bundle flow, and the second one the upward flow, through the central large tube, to the cold trap outlet. A one-dimensional description is employed for the tube flow and a zero-dimensional description for the shell (i.e., lumped approach). The geometry of the test section itself is simplified through a number of approximations.

The tube-bundle flow is simulated by a downward flow through a circular vertical tube of hydraulic diameter $d_h = 11$ mm and length $L = 183$ mm. The gas temperature and the flow mass velocity at the inlet section are set equal to the experimental conditions. Hence, the first computational cell models average conditions over the tube-bundle cross-section. The second calculation cell consists of a circular tube 24 mm in diameter, whose length is again taken equal to 183 mm. The complicated two-phase heat transfer problem in the shell is not considered in its details. Instead, the shell is modelled as a perfectly isothermal medium, both axially and radially, containing a fluid of an extremely high heat capacity. Accordingly, a constant temperature condition is assumed to prevail at the tube wall surface. The basis for this idealization is that relatively small differences were found between the temperature measurements performed in the shell. In all the studied cases the length of 183 mm largely exceeded the thermal entrance length, therefore, the gas exits from the first and enters into the second computational cell with a temperature equal to the value specified at the wall. For this reason, the second calculation has been always found to alter minimally the end conditions predicted by the first computation cell.

The flow was laminar (the Reynolds number at the entrance was approximately 50). Hydrodynamic

entrance effects are neglected. Axial diffusion in the flow is neglected as well. The associated Péclet number was approximately 35. For this value, the results of Schmidt and Zeldin [8] indicate that axial diffusion has a noticeable influence over a length of one diameter. By ignoring the above two effects, no significant error is introduced in the calculation of the exit conditions, considering the length of the tube. Near the inlet section, instead, the predicted values will contain higher errors. Still, however, this is acceptable for our modelling purposes, which focus on relative comparisons between parameters, rather than on their absolute magnitude.

The Grashof number is of the order of 10^4. According to the Metais and Eckert flow regime chart for vertical tubes, the flow is found to be in the mixed convection regime. Considering that the problem deals with cooling in downward flow, the superimposed buoyancy will tend to flatten the velocity profile by accelerating the fluid near the wall, and, hence, to enhance heat and mass transfers. In the calculations two separate cases were considered: a fully developed forced convection, where a parabolic velocity profile is assumed, and a buoyancy-distorted velocity distribution, where a radially uniform velocity profile is assumed (plug flow). The classical mass transfer data of Linton and Sherwood support the idea that the superimposed free convection may be reasonably accounted for by considering a flat velocity profile (see, for example, ref. [9]). Finally, given the low water vapour concentrations employed, latent heat released by condensation and nucleation is neglected, thereby decoupling the heat transfer from the mass transfer problem.

Thermodynamic data for the water vapour pressure over ice were taken from ref. [10]. The transport properties of the water vapour–air mixture are calculated from the standard formulae of the kinetic theory of gases. Aerosol particles were assumed to be spherical. Since particle sizes are predicted to be small, particle velocities are approximated to be equal to the carrier gas velocity. Their bulk density was taken equal to that of ice at 0°C ($\rho_p = 913$ kg m^{-3}). A separate sensitivity study showed that the modelling results are practically independent of the value assigned to this parameter.

The main processes are modelled by a set of integrodifferential equations. In what follows we present the model equations in the form they take for constant cross section.

The first equation, which determines the carrier gas velocity, is the mass continuity equation for the carrier gas

$$\frac{\partial \rho_g}{\partial t} + \frac{\partial}{\partial x}(u_g \rho_g) = 0. \tag{1}$$

In the above equation the density ρ_g is obtained from the ideal gas law.

The second equation describes water-vapour transport and its depletion due to homogeneous nucleation, condensation onto particles (growth term), and diffusion to the cold structural surfaces (wall condensation). It is expressed as follows

$$\frac{\partial C_v}{\partial t} + \frac{\partial}{\partial x}(u_g C_v) = -\frac{4\,Sh\,D_v}{d_h^2}(C_v - C_{wall}) - \frac{4}{3}\pi\rho_p (r^*)^3 J_{nucl} - 4\pi\rho_p \int_0^\infty r^2 \dot{r} n \, dr. \tag{2}$$

The first term on the right of equation (2) is the condensation rate onto the wall surfaces which is expressed in terms of the apropriate mass transfer coefficient. In this formulation, the concentration C_{wall} is taken equal to the saturation value at the wall temperature. The second term is the condensation rate due to homogeneous nucleation, and the third term arises from particle growth due to vapour condensation onto pre-existing particles.

The condensed matter concentration in the flow (ice particles) is calculated by integrating the particle size distribution over the whole size spectrum:

$$C_p = \frac{4}{3}\pi\rho_p \int_0^\infty r^3 n \, dr. \tag{3}$$

The aerosol size distribution is determined from the solution of the aerosol general dynamic equation for the particle number probability distribution,

$$\frac{\partial n}{\partial t} + \frac{\partial}{\partial x}(u_g n) + \frac{\partial}{\partial r}(\dot{r} n) = I_{coag} + J_{nucl}\delta(r - r^*) - \frac{4}{d_h} v_d n. \tag{4}$$

The third term on the left of equation (4) gives the particle growth rate due to condensation onto particles (gas-to-particle conversion), while the first term on the right results from particle collisions, the second term arises from homogeneous nucleation, and the last term gives the rate of particle removal due to surface deposition.

Below, an account is given of the modelling of the various source/sink terms appearing in the previous equations. All of them are calculated from standard expressions used in aerosol dynamics, and, thus, their detailed form is not reproduced.

The homogeneous nucleation rate J_{nucl} and the critical embryo size r^* are calculated according to classical nucleation theory (see, for example, ref. [11]). Previous studies suggest that the classical nucleation theory underpredicts the nucleation rate in tube flow [5]. The homogeneous nucleation rate is expected to be further underestimated, owing to the one-dimensional approach employed. The Lewis number for water vapour–air mixtures is less than unity ($Le \approx 0.85$). This implies that particles will first start to form close to the wall, rather than in the bulk of the flow [6, 12]. This effect cannot be replicated by a one-dimensional approach, which requires the whole cross-section to be brought to a high supersaturation prior to any

onset of nucleation takes place. Discrepancies between modelling and experimental results are, therefore, expected in the region in which ice particles start to appear in the flow.

The growth rate $\dot{r}$ is determined from the expression derived by Fuchs and Sutugin [13] that reproduces the standard expressions for particle growth in the diffusion regime and in the free-molecular regime.

The particle coagulation integral I_{coag} accounts only for the collisions due to Brownian motion. This is calculated according to the expression suggested by Hidy and Brock [14]. Collisions due to gravity and shear are neglected.

The deposition velocity v_d is given by the addition of the velocities corresponding to the two mechanisms of interest, namely, thermophoresis and Brownian diffusion. The thermophoretic deposition velocity is calculated from the Springer equation [15]. Brownian deposition velocity is inferred from the particle diffusion coefficient and the associated Sherwood number. Among the two mechanisms, thermophoresis is the dominant one for the removal of the ice particles from the flow. The thermophoretic deposition velocity depends on the local radial temperature gradient which, in the one-dimensional approximation, is evaluated in terms of the thermal boundary-layer width and the bulk-gas to wall-temperature difference, $\Delta T = T_g - T_{wall}$. This approximation is reasonable because thermophoresis will occur downstream the nucleation zone where ΔT will be relatively small. Previous modelling work has shown that for small ΔT the one-dimensional approach predicts satisfactorily the thermophoretic deposition [16].

To close the system of the model equations, the knowledge of the gas bulk temperature T_g and of the local Sherwood number Sh in the entrance region of the tube is required. Assuming steady-state conditions, T_g and Sh are obtained from the numerical evaluation of the Graetz series solution. For the case of the parabolic velocity profile the eigenvalues and the related constants are calculated from the formulae suggested by Shah and London [17]. In the plug flow case, the series solution involves the zeros of Bessel functions (see, for instance in [9]). These were obtained from the tables and asymptotic formulae available in [18].

The one-dimensional Lagrangian code developed by Im *et al.* [7] is used to solve numerically the coupled integro-differential equations. Details on the numerical aspects can be found in ref. [19]. The numerical scheme, which was found very stable numerically and computationally inexpensive, is based on a marching forward integration procedure and it uses a varying axial grid. This is required because a fine axial mesh has to be placed at the location in the tube where nucleation (which implies a shock-wave like change in the solution) will occur. At any location X, an axial step ΔX is predicted from current information, and if any variable calculated at $X+\Delta X$ changes more than allowed, then the calculation is repeated by correcting the step size to $\Delta X/2$. The maximum allowable change across a ΔX is specified separately for each variable by considering its sensitivity. For instance, for the supersaturation ratio the maximum change was set to 0.05 (absolute), whereas for the mass condensed by particle growth the maximum change was set to 0.1 (fractional). In solving equation (4), an additional discretization in r is used that is applied over a fixed particle-size grid. This grid has been defined so that the range from 5×10^{-4}–35 μm is logarithmically divided into 64 size intervals. Since the experiments were performed under steady-state conditions the steady-state solution of the equations was calculated numerically.

5. RESULTS AND DISCUSSION

Figures 3(a) and (b) show the results from two experimental runs, which were both carried out under the reference inlet conditions [i.e., $\dot{m}_{in} = 1$ m^3 (STP)/h, $C_{in} = 1250$ ppm]. In Fig. 3(a) the data are presented

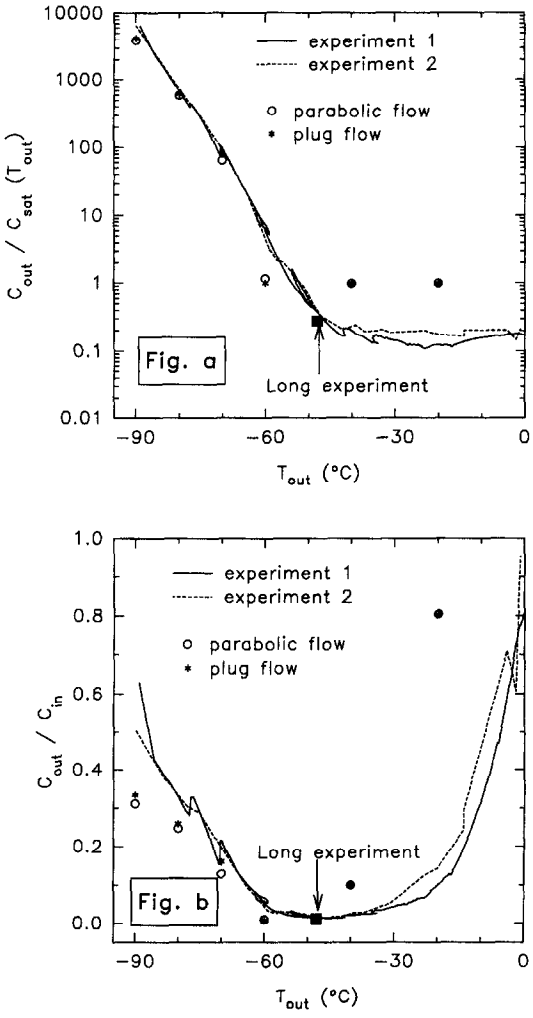

Fig. 3. Experimental and modelling results for the reference case [$\dot{m}_{in} = 1$ m^3 (STP)/h, $C_{in} = 1250$ ppm].

in terms of relative humidity at the outlet [$C_{out}/C_{sat.}(T_{out})$] vs. exit gas temperature, whereas Fig. 3(b) shows the ratio of the outlet to the inlet water content (C_{out}/C_{in}). The following general behaviour is observed: down to some temperature (of about $-50°C$), the trapping efficiency is found to be acceptable in that the exit stream is undersaturated. At lower temperatures the efficiency deteriorates and the gas leaves the trap supersaturated. A further temperature reduction does not improve the situation. Instead, it is accompanied by an increased moisture breakthrough. The increased water content at the exit is due to the transport of frozen particles to the outlet. As will become apparent below, for temperatures warmer than $\approx -50°C$ there is no particle formation in the flow and moisture removal is exclusively performed through wall condensation. Hereafter this regime will be referred to as all-vapour regime. For colder temperatures, ice particles are present in the flow that drastically limit diffusional transfer to the wall. This regime will be subsequently referred to as particles-and-vapour regime.

Figures 3(a) and (b) demonstrate that the repeatability of the experimental data is satisfactory. Given the experimental procedure employed, the transient behaviour of the runs was not the same. However, as can be seen in the figures, the agreement between the experimental results is good, suggesting that the assumption of stationary conditions during the tests is satisfied. Moreover, a long-lasting experimental run has been performed during which temperature conditions were kept stable over a period of approximately 12 h. The obtained experimental point, shown in Fig. 3 as the solid square symbol, coincides with the data obtained from the shorter tests. This result corroborates our assumption that the data from the shorter experiments refer to steady-state conditions.

In Figs. 3(a) and (b) the model predictions are also plotted for the two different velocity profiles used (parabolic and uniform). As discussed earlier, the numerical simulations assume that the exit gas temperature and the wall temperature yield the same value. Thus, the modelling results may also be viewed as being plotted against the wall temperature. Notwithstanding some noticeable differences between experimental data and model predictions, the model reproduces correctly the dominant behaviour of the experiment. Namely, the model predicts an initial increase of the efficiency with decreasing wall temperature down to about $-60°C$; a subsequent wall-temperature decrease reverses the trend and the efficiency decreases. Note also that the assumption regarding the velocity profile has only a minor influence on the calculations.

A closer comparison between the experimental and numerical results shows that the model performs quite satisfactorily in the particles-and-vapour regime. The transition from the all-vapour regime [defined grossly, as the minimum of the curve in Fig. 3(b)], is predicted at a wall temperature of $-60°C$. This result is in acceptable agreement with the observed value of $\approx -50°C$. The reason that the simulations require a lower temperature to initiate the particles-and-vapour regime may be partly attributed to the use of a one-dimensional approach which, as discussed in the previous section, underpredicts the nucleation rate.

The predictions in the all-vapour regime overestimate markedly the observed exit humidities. The tube is long enough, so the model predicts always a water vapour concentration at the exit, equal to the saturation vapour concentration corresponding to the wall temperature. The experimental data show, instead, that in this zone, the exit stream is always undersaturated. In investigating this effect the possibility that the vapour phase and the condensate are not in thermodynamic equilibrium at the wall surface was first addressed. The basis for such an assumption is that, due to the small amounts of vapour used, the condensate, especially at the beginning of the experiment, may form only a few molecular layers, thereby, not behaving like a continuum. With increasing time, however, as the layers build up, the non-equilibrium features must disappear. This prerequisite was not supported by any experimental evidence: in the long-lasting experimental run, over a period of more than 12 h, the exit gas temperature and exit dew-point temperature remained quite stable (well within two standard deviations), without exhibiting any trend towards convergence, i.e., towards establishing a saturation state. On the basis of this remark, the assumption of initially non-equilibrium deposition has to be discarded. The most plausible explanation for the unsaturated stream at the exit, is that radial temperature inhomogeneities over the cross-section of the tube-bundle (i.e., cold and hot spots) are not negligible. Although the two available measurements in the shell indicate small temperature variations along the shell height, the possibility of radial variations cannot be excluded. Actually, these variations need not necessarily be pronounced. Owing to the exponential relationship between saturation pressure and temperature, even moderate radial inhomogeneities may induce a significant effect at the exit of each individual tube of the bundle. To simulate the effect, an appropriate model for predicting the radial temperature variation in the shell is needed.

The model predictions provide us with insights on the mechanisms that determine the efficiency of the cold trap. The predictions may be interpreted by considering the competition between wall condensation and particle formation and growth. Figure 4 shows in detail the numerical results obtained with the reference conditions at three different wall temperatures. The results are shown as a function of the axial location X, up to $X = 183$ mm (i.e., up to the exit of the tube-bundle). As mentioned in the previous section, the computation of the rising part of the flow leaves the results practically unchanged.

Four variables are plotted: the supersaturation

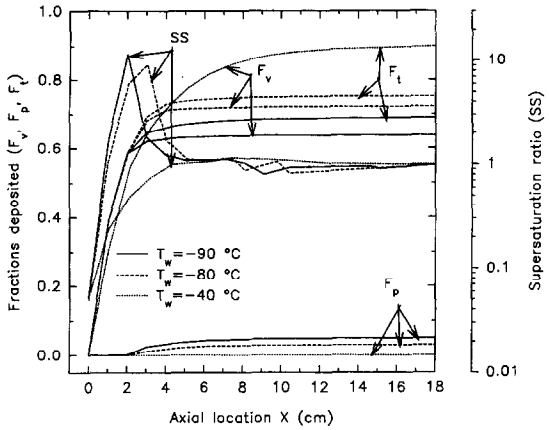

Fig. 4. Effect of wall temperature at $\dot{m}_{in} = 1$ m^3 (STP)/h, and $C_{in} = 1250$ ppm. Calculated supersaturation ratio (SS) and deposited fractions (F_v, F_p, F_t) as functions of axial location.

ratio, defined in the usual way in the one-dimensional approximation,

$$SS = \frac{\text{vapour bulk average concentration}}{\text{saturation concentration at the gas bulk temperature}} \quad (5)$$

the fraction deposited as vapour,

$$F_v = \frac{\text{vapour mass flux to the wall, integrated from 0 to } X}{\text{vapour mass flow rate at the inlet section}} \quad (6)$$

and the fraction deposited as particles,

$$F_p = \frac{\text{particle mass flux to the wall, integrated from 0 to } X}{\text{vapour mass flow rate at the inlet section}}. \quad (7)$$

Clearly, the total fraction deposited F_t is $F_v + F_p$.

At −40°C (a temperature that falls within the all-vapour regime) the model effectively predicts no particle formation, and deposition is due to vapour condensation on the structures. Total deposition coincides with wall condensation in this case, and it is the highest of all three cases, demonstrating that vapour condensation is a more efficient removal mechanism that particle deposition. At these conditions the cold trap is an efficient device to remove water vapour from the carrier gas.

The other two cases, at −80 and −90°C, correspond to the particles-and-vapour regime. Here, the model effectively predicts particle formation in both cases. Inspection of the supersaturation ratios shows that at colder wall temperatures (−90°C) particle formation occurs closer to the tube inlet. The reason is that gas temperature, and, hence, the saturation pressure drop off more rapidly in this case. Relative particle deposition is higher at the lower temperature but the main difference in the efficiency arises from differences in vapour deposition. Vapour deposition is considerably higher for the higher temperature (−80°C) primarily because particle formation occurs further away from the tube inlet, thereby allowing a larger region for wall condensation. In agreement with the experimental results, total relative deposition is higher at the higher temperature. A similar temperature effect has also been reported in a previous work, which dealt with cesium vapour condensation in laminar argon flow [20]. Finally, we note that the calculations predict particle number concentrations at the exit of the order of 10^5 particles cm^{-3} and particle radii in the range of 1 to 2 μm.

Clement [12] has extensively analyzed the coupled heat, mass transfer equations and their coupling to the aerosol size distribution. He shows that the aerosol condensation rate and the wall condensation rate depend on a dimensionless number, Cn, which he calls the condensation number. The condensation number grows rapidly with decreasing wall temperature (for $T_{wall} = -80$°C, $Cn \approx 2 \times 10^4$). The analysis shows that for $Le < 1$ and $Cn \gg 1$, the proportion of vapour which condenses onto particles becomes very large. The modelling results reproduce successfully this effect. Figure 4 shows that immediately after the nucleation front diffusional losses to the wall are inhibited (the vapour deposition curves reach a plateau). Downstream the onset of nucleation, the available water vapour is depleted by particle growth and at the expense of wall condensation. Particles, therefore, act as a shield to vapour diffusion to the wall, and, hence, they facilitate humidity transport to the device outlet. This is the basic effect that is responsible for the deterioration of the efficiency of the process.

A series of additional experiments was performed to investigate a number of parametric effects. The significance of heterogeneous nucleation on pre-existing aerosol particles was investigated using two different carrier gases. One carrier was delivered by the compressed air network of the laboratory and, hence, contained atmospheric aerosol particles, while the other one was a particle-free carrier supplied from a pure atmospheric air gas bottle. The effect was not found to be important. This conclusion may be also indirectly drawn on the basis of the repeatability of the tests carried out using the compressed air network. The aerosol characteristics in the compressed-air carrier are random, depending on the atmospheric conditions and the particular state of the network during the test. The fact that the same experimental results are obtained indicates that condensation on pre-existing aerosols has a negligible effect. A possible explanation is that the concentration of these particles is below the limit required to suppress homogeneous nucleation of embryos. Previous studies on laminar tube flow suggest this limit to be between 10^3 and 10^7 particles cm^{-3} [4, 5], hence, close to the typical value of particle number concentration in the atmosphere (10^4 particles cm^{-3}; see, for example, ref. [10]).

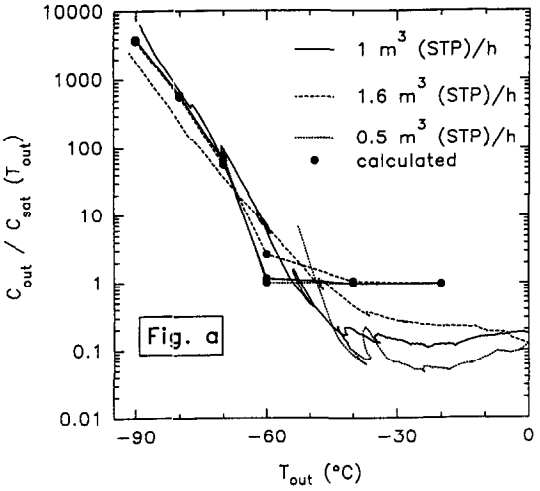

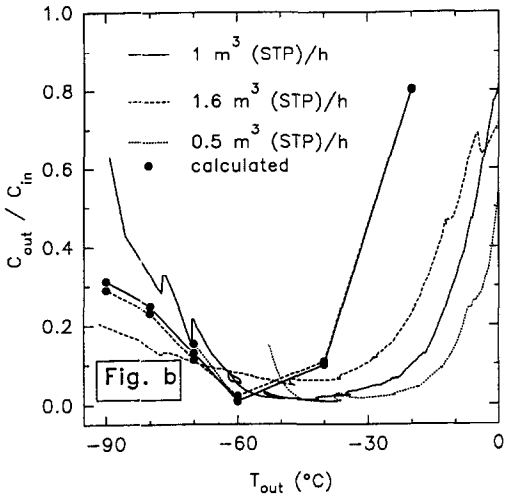

Fig. 5. Experimental (lines) and modelling (lines with dots) results with various mass flow rates at $C_{in} = 1250$ ppm.

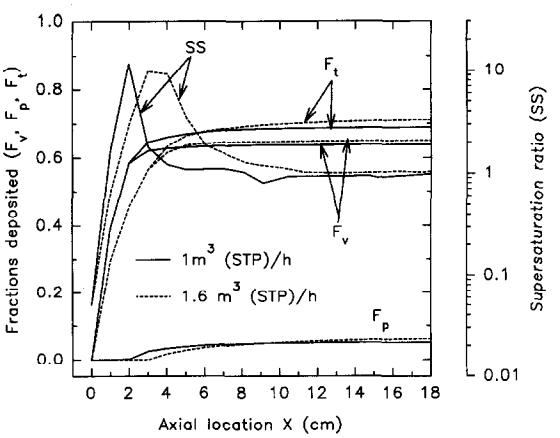

Fig. 6. Effect of mass flow rate at $T_{wall} = -90°C$ and $C_{in} = 1250$ ppm. Calculated supersaturation ratio (SS) and deposited fractions (F_v, F_p, F_t) as functions of axial location.

The parametric effect of the mass flow rate is shown in Fig. 5, where the data from three experiments performed with different flow rates are plotted together. In the all-vapour region the results show that the humidity at the exit increases with the flow rate. As in the reference case, the exit stream is always undersaturated. The model calculations (also shown in Fig. 5), predict saturation at the exit, and hence, do not display any flow rate dependence. Here again, the observed flow rate effect can be attributed to radial wall-temperature inhomogeneities in the tube-bundle. With a larger flow rate, the radial variations over the cross-section of the tube-bundle become less pronounced, hence, the exit humidity becomes closer to the saturation state corresponding to the mean exit temperature.

In the particles-and-vapour regime, the exit humidity continues to depend on the flow rate, but the trend is opposite to that discussed previously, the higher values corresponding to the lower flow rates. The model calculations reproduce this trend, though, the predicted dependence is smaller than the observed. The explanation for the flow rate effect may be deduced from Fig. 6, which presents simulation results with two flow rates, at a wall temperature of $-90°C$. The plot of the supersaturation ratio shows that at the lower flow rate supersaturation occurs closer to the inlet and exhibits a sharper peak. This is consistent with the remark that at a smaller flow rate, the gas is cooled more efficiently and its temperature drops more abruptly. Consequently, the onset of nucleation takes place closer to the inlet and the region where wall condensation prevails is correspondingly reduced. In fact, the vapour deposition curves in Fig. 6 show that vapour deposition is slightly lower at the lower flow rate. Moreover, particle deposition is predicted to be slightly lower at the smaller flow rate. This effect is connected to lower thermophoretic deposition, due to smaller temperature differences between the gas and the wall (as mentioned earlier, cooling is enhanced with the lower flow rate). The overall result is that at the lower flow rate, lower humidity removal is achieved.

The parametric effect of the inlet humidity is shown in Fig. 7, where experimental and numerical results from two runs performed at the same mass flow rate but with different inlet humidities (625 and 1250 ppm) are plotted together. In the all-vapour regime, the experimental data suggest a dependence on the inlet humidity, namely increased efficiency with increasing inlet humidity, especially at temperatures lower than $-15°C$. The model predicts similar dependence, which arises from the simple fact that at a given wall temperature C_{out} remains unchanged (and equal to C_{sat}); hence, the ratio C_{out}/C_{in} becomes inversely proportional to the inlet humidity.

In the particles-and-vapour regime, both experimental and calculational results show that the ratio of outlet to inlet humidity decreases with decreasing inlet humidity. A similar effect has been also observed

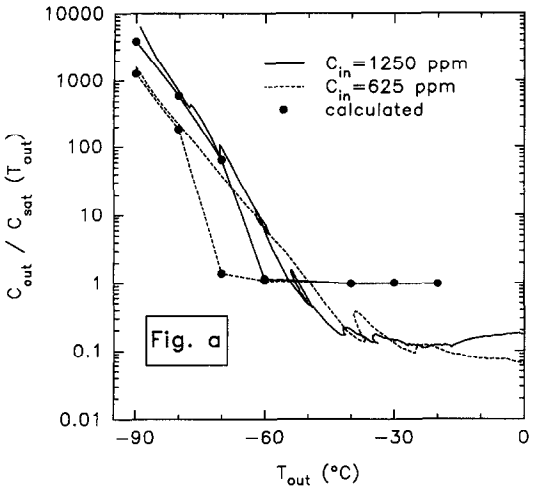

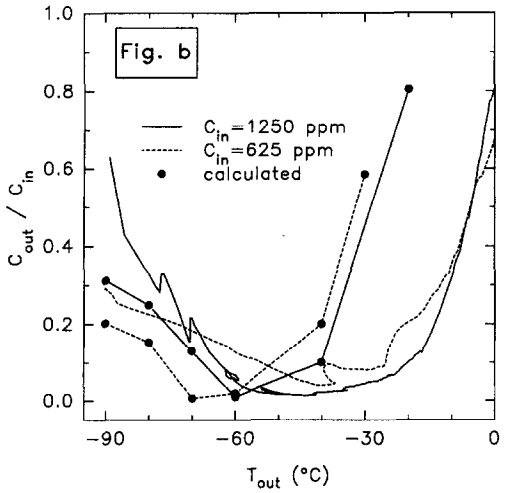

Fig. 7. Experimental (lines) and modelling (lines with dots) results with two different inlet humidities at $\dot{m}_{in} = 1$ m^3 (STP)/h.

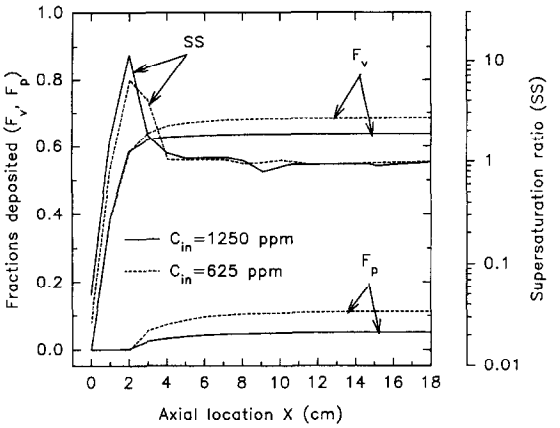

Fig. 8. Effect of inlet humidity at $T_{wall} = -90$°C and $\dot{m}_{in} = 1$ m^3 (STP)/h. Calculated supersaturation ratio (SS) and deposited fractions (F_v, F_p) as function of axial location.

in [20]. The detailed numerical results of the simulations at −90°C are given in Fig. 8. The model predicts that the value of the maximum supersaturation ratio depends on the inlet humidity (decreasing value with decreasing inlet humidity), but homogeneous nucleation starts at the same position. Vapour deposition is predicted to be higher at the lower inlet humidity because the supersaturation peak is more spread out. Particle deposition is predicted to be higher, as well. The calculations show that the particle sizes are smaller when the inlet humidity is lower (at the exit, the mass-mean radius is 0.57 μm, against a radius of 1.2 μm obtained in the higher humidity case). The calculated trend in the particle sizes, is in agreement with predictions from more elaborate theoretical analyses [4]. Hence, Brownian diffusion is more efficient in the low humidity case and it becomes the distinguishing deposition mechanism (thermophoresis is not very sensitive on particle size).

6. CONCLUSIONS

An experimental and modelling investigation has been carried out to study the efficiency of a cold trap to remove low concentration water vapour from air. The experimental test section consists of a tube-bundle of 57 vertical tubes, accommodated in a cryogenic shell. The emphasis of the study is placed on the influence of the temperature on the efficiency of the process. The effects of some other experimental parameters, such as inlet humidity and mass flow rate, were also considered to investigate the sensitivity of the experimental results and to check the performance characteristics of the model.

Since the experiment was designed to determine the overall efficiency of the cold trap, it seemed reasonable to adopt a simple modelling approach to obtain a tool for the interpretation of the experimental results, rather than to quantify detailed microphysics. The model, which is based on a one-dimensional approach, represents the test section through simplifying idealizations, and it uses standard expressions for aerosol dynamics. It incorporates, however, two noteworthy elaborations. The particle population, rather than taken to be monodisperse, is described through the whole size spectrum; and the heat and mass transfer entrance effects are described by the analytical expressions of the Graetz problem.

The experimental results show that an optimal temperature range exists for the operation of the cold trap. This behaviour can be attributed to the competition between wall condensation and particle formation and growth. The process can be described as follows: due to a sharp drop in the saturation pressure with gas cooling, a nucleation front occurs at some axial location, dividing the flow into two zones. In the upstream zone the removal mechanism is vapour diffusion to the structural walls, while downstream vapour is depleted almost exclusively by the formation and growth of ice particles that are transported to the

outlet of the device. Therefore, the overall removal efficiency is determined, mainly, by the length taken up by the upstream zone. Under certain temperature conditions, this zone covers the whole tube (i.e., no nucleation occurs) and, thus, enhanced removal efficiency is achieved. This corresponds to the optimal temperature range observed. When temperature is further lowered, the upstream length becomes progressively shorter with decreasing temperature, and, thus, a reversion in the behaviour of the process is observed. In the present experimental conditions, optimal trapping efficiency was obtained at an exit gas temperature of about $-50°C$, and was associated with the removal of 98.89% of the humidity inflow.

The model reproduced correctly the observed dependence of the trapping efficiency on temperature. In particular, it confirmed the existence of an optimal operational temperature range. Considering its simplicitly, it gave predictions in reasonable agreement with the experimental data over half of the studied temperature range (in the zone of the colder temperatures). For the warmer temperatures, the simulations overpredicted substantially the experimental results. The origin of these discrepancies is attributed to the presence of non-negligible temperature inhomogeneities over the cross-section of the tube-bundle.

With respect to parametric effects, we found that an increase of the mass flow rate improved the trapping efficiency over the range of the colder temperatures. Here again, this effect can be interpreted in terms of the length over which removal is undertaken by vapour diffusion to the wall. A decrease of the inlet vapour concentration was found to result in a similar efficiency improvement. In this case, the effect can be attributed to the formation of smaller ice particles.

The whole analysis makes reference to general concepts of aerosol formation in tube flow, without recognizing particular features of the condensed phase. It may be reasonably inferred that the approaches developed to describe significantly different systems (i.e., gas–liquid aerosol flows at much higher temperatures) may be extrapolated to the case of a water vapour–air mixture at temperatures substantially below 0°C.

Acknowledgements—The work has been performed within the framework of the 1992–94 European Fusion Technology Programme (Task EC-T48.8). The authors would like to thank Dr M. Lazaridis and Dr A. J. Hautojarvi for useful discussions held during the development of the study.

REFERENCES

1. O'Hira, S., Konishi, S., Naruse, Y., Okuno, K., Barnes, J. W., Harbin, W., Bartlet, J. R. and Anderson, J. L., Test of the cold traps in the JAERI fuel cleanup system in the Tritium Systems Test Assembly, JAERI-M 93-087 Japan Atomic Energy Research Institute, Ibaraki-ken, Japan, 1993.
2. Chabot, J., Fernadez de Grado, G. and Herry, P., Cold trap development. Task TCP 3-1, SCECF 303, Commissariat à l'Energie Atomique, Fontenay-aux-Roses, France, May 1993.
3. Fukada, S., Furata, S. and Mitsuishi, N., Mass transfer with mist formation for laminar flow in vertical cooling tube with constant temperature wall. Experimental and theoretical study on fuel gas refining system with cryogenic freezer. *Nippon Genshiryoku Gakkaishi*, 1989, **31,** 487–496 (In Japanese).
4. Pesthy, A. J., Flagan, R. C. and Seinfeld, J. H., The theory of aerosol formation and growth in laminar flow. *Journal of Colloid Interface Science*, 1983, **91,** 525–545.
5. Nguyen, H. V., Okuyama, K., Mimura, T., Kousaka, Y., Flagan, R. C. and Seinfeld, J. H., Homogeneous and heterogeneous nucleation in a laminar flow aerosol generator. *Journal of Colloid Interface Science*, 1987, **119,** 491–504.
6. Barret, J. C. and Fissan, H., Wall and aerosol condensation during cooled laminar tube flows. *Journal of Colloid Interface Science*, 1989, **130,** 498–507.
7. Im, K. H., Ahluwalia, R. K. and Chuang, C. F., RAFT: a computer model for formation and transport of fusion product aerosols in LWR primary system. *Aerosol Sci. Technol.*, 1985, **4,** 125–140.
8. Schmidt, F. W. and Zeldin, B., Laminar heat transfer in the entrance region of ducts. *Appl. Sci. Res.*, 1970, **23,** 73–94.
9. Skelland, A. H. D., *Diffusional Mass Transfer*, Chap. 5. Wiley, New York, 1974.
10. Rogers, R. R. and Yau, M. K., *A Short Course in Cloud Physics*, 3rd edn, Chaps. 2 and 9. Pergamon Press, Oxford, 1989.
11. Friedlander, S. K., *Smoke, Dust and Haze*, Chap. 9. Wiley, New York, 1977.
12. Clement, C. F., Aerosol formation from heat and mass transfer in vapour–gas mixtures. *Proceedings of the Royal Society of London*, 1985, **A398,** 307–339.
13. Williams, M. M. R. and Loyalka, S. K., *Aerosol Theory and Practice*. Pergamon Press, Oxford, 1991, p. 249.
14. Hidy, G. M. and Brock, J. R., *The Dynamics of Aerocolloidal Systems*. Pergamon Press, Oxford, 1970, pp. 308–309.
15. Springer, G. S., Thermal force on particles in the transition regime. *Journal of Colloid Interface Science*, 1970, **34,** 215–220.
16. Hontañón, E., Lazaridis, M. and Drossinos, Y., The effect of chemical interactions on the transport of caesium in the presence of boron. *J. Aerosol Sci.*, 1996, **27,** 19–39.
17. Shah, R. K. and London, A. L., *Laminar Flow Forced Convection in Ducts*, Chap. V. Academic Press, New York, 1978.
18. Abramowitz, M. and Stegun, I. A., *Handbook of Mathematical Functions*, Chap. 9. NBS Applied Mathematics Series 55, 1972.
19. The RAFT computer code for calculating aerosol formation and transport in severe LWR accidents, NP-5287-CCM, Electric Power Research Institute, Palo Alto, California, July 1987.
20. Borishanskiy, V. M., Paleyev, I. I., Arefýev, K. M., Ivashchenko, N. I., Zablotskaya, T. V., Khomchenkov, B. M. and Fishman, N. M., Condensation of cesium vapor from a flow of argon. *Heat Transfer—Soviet Research*, 1972, **4,** 87–93.